Ab initio self-consistent calculations of the Compton profiles and polarizabilities of diamond and cubic boron nitride

1998 J. Phys.: Condens. Matter 10 557

(http://iopscience.iop.org/0953-8984/10/3/009)

J. Phys.: Condens. Matter **10** (1998) 557–575. Printed in the UK PII: S0953-8984(98)82539-3

Ab initio self-consistent calculations of the Compton profiles and polarizabilities of diamond and cubic boron nitride

David Ayma, Michel Rérat and Albert Lichanot

Laboratoire de Chimie Structurale, UMR 5624, Université de Pau, IFR, rue Jules Ferry, 64000 Pau, France

Received 13 March 1997, in final form 28 August 1997

Abstract. Compton profiles, polarizabilities and related functions of diamond and cubic boron nitride have been investigated within the Hartree–Fock approximation and the density functional theory, calculated within the local density approximation and generalized gradient approximation, but without any explicit correlation correction for the Compton profiles. The correlation part already included in the standard uncorrected density functional theory is deduced from the comparison of the two types of calculation. The Compton profile and reciprocal-form-factor anisotropies, polarizability, dielectric constant and energy loss function of the two compounds are compared at the same level of accuracy. These properties are very close in spite of the rather different chemical bonds due to the charge transfer occurring in cubic boron nitride and gaps.

1. Introduction

Since its synthesis in 1957 by Wentorf [1], cubic boron nitride (cBN) has attracted particular attention because of its extraordinary properties of technological interest. The electronic properties, due to its large band gap, have applications in modern microelectronic devices working under high temperatures, whereas its mechanical properties make it useful for protective coatings. It is used both as a powerful material for abrasive processes and a sintered one when inserted in high-speed equipment for machining hardened steels. Diamond and cBN are isoelectronic and isostructural (zinc-blende-type structure) compounds but the space-group symmetry is changed from the centrosymmetric $F_{d\bar{3}m}$ group for diamond to the non-centrosymmetric $F_{\bar{4}3m}$ one for cBN. As a consequence of these similarities, diamond and cBN have been studied comparatively in detail from an experimental point of view as well as by means of theoretical investigations. Concerning their electronic structure, to which this paper is devoted via calculations of Compton profiles, numerous studies on the x-ray diffraction, Compton scattering, charge-density distribution, and total and cohesive energies of the ground state have already led to accurate and homogeneous results. Experiments on diamond [2–5] and cBN [6–9] and calculations performed on diamond [10–18] and cBN [19–26] either with the Hartree–Fock (HF) or the Kohn–Sham (KS) equations have been used to determine an accurate description of their electronic structure.

Ab initio calculations of the crystalline wave functions of diamond and cBN already made by Dovesi *et al* [15, 21] and Orlando *et al* [22] at the HF level only, with either a minimal STO-3G basis set or a more extended 6-21G* set, are improved on in this work. In fact, the linear combination of atomic orbitals (LCAO) self-consistent-field (SCF) method applied to the periodic systems [27] and implemented in the program CRYSTAL [28],

0953-8984/98/030557+19$19.50

was available within the HF approximation. Recently, a new version of this program, CRYSTAL 95 [29], has allowed us to benefit from important improvements and in particular to use the density functional theory (DFT) formalism thanks to the resolution of the Kohn–Sham (KS) one-electron equations at each step of the SCF process. In these conditions, the charge and momentum densities obtained from the eigenvectors calculated at the HF and KS levels can be compared, thus leading to the evaluation of a part of the correlation effect. These improvements also allow us to establish more accurately properties such as the polarizability which require knowledge of the gap and the conduction band. This latter property, which is the linear response of an electronic system to the application of an electric field, is a complex function for which the real and imaginary parts are related via the Kramers–Krönig relation [30, 31]. The dielectric constant which is the corresponding macroscopic property is involved in basic experiments such as optical measurements of the refractive index or reflectance [32] and electron energy loss spectroscopy (EELS) [33–35]. To calculate the polarizability and its related functions, the uncoupled Hartree–Fock (UCHF) or uncoupled Kohn–Sham (UCKS) schemes already described [36] are used.

The paper is organized as follows. In section 2 the calculation of the crystalline wave functions within the DFT formalism is briefly recalled and the atomic basis sets used are reported. In section 3, the equations required for the calculations of the properties studied are summarized. Section 4 reports calculations made at the HF and KS levels, and the part of the electronic correlation effect included in standard uncorrected DFT is evaluated for each property. The comparison with experiment and other calculations is also analysed. Finally in section 5, the comparative behaviour of the Compton profiles, polarizabilities and related functions for diamond and cBN are discussed in connection with the nature of the chemical bonds and the gap and bandwidth values, and general conclusions are given in section 6.

2. Details of the calculations of the wave function

The periodic LCAO-HF scheme [27] as implemented in the CRYSTAL 92 program [37] is used. The accuracy of calculating the Coulomb and exchange series contributions to the Fock operator is addressed by setting tight tolerances [28] for the evaluation of these series ($S_c = t_m = 10^{-6}$ and $S_{ex} = p^g_{ex} = 10^{-6}$, and $p^l_{ex} = 10^{-12}$). The shrinking factor defining the reciprocal-space net in which the Fock matrix is diagonalized is 8 corresponding to 29 (diamond) and 43 (cBN) reciprocal-space k-points. With these computational conditions, the converged total energy is obtained with an accuracy of about 0.1 mHartree. For C, B and N atoms, we used the all-electron gaussian basis sets (6-21G*) given by Orlando *et al* [22] in the study of diamond and cBN semiconductors. The use of such basis sets is justified since it allows us to compare the Compton profiles of diamond and cBN without including basis set effects. Moreover, the quality is judged as sufficient since the calculations of the Compton profiles for hexagonal BN [38] made with this basis set (B^*_1 in reference [38]) are similar to those obtained with a more extended basis set (7-311G*; B^*_2 in reference [38]). In order to compare our calculated properties more accurately with the experimental ones, we have reoptimized the exponent (ξ) of each outermost (3sp) shell with respect to the experimental geometry (3.560 Å for diamond; 3.615 Å for cBN). This process leads to the following values: $\xi(\mathrm{C}) = 0.2242$, $\xi(\mathrm{B}) = 0.1843$ and $\xi(\mathrm{N}) = 0.3132$. A d-like polarization function with the exponent $\xi = 0.8$ was added to the basis set of each atom.

Parallel to the LCAO-HF method, we have been able to make LCAO-KS calculations thanks to the recent extension of the CRYSTAL code to the DFT [39, 40]. This allows a direct comparison between HF and DFT methods using the same code, the same basis

sets and the same computational conditions. In this CRYSTAL code, the HF and KS one-electron equations are solved self-consistently for a one-electron wave function, and the corresponding electronic density $\rho(\boldsymbol{r})$ is calculated:

$$\hat{H}_{\mathrm{HF/KS}}\varphi^{\boldsymbol{k}}_{i\,\mathrm{HF/KS}} = \varepsilon^{\boldsymbol{k}}_{i\,\mathrm{HF/KS}}\varphi^{\boldsymbol{k}}_{i\,\mathrm{HF/KS}} \tag{1}$$

$$\rho_{\mathrm{HF/KS}}(\boldsymbol{r}) = \sum_{\mu,\nu,\boldsymbol{g}} P^{\mu,\nu,\boldsymbol{g}}_{\mathrm{HF/KS}}\chi^{\boldsymbol{0}*}_{\mu}(\boldsymbol{r})\chi^{\boldsymbol{g}}_{\nu}(\boldsymbol{r}) \tag{2}$$

where $\varphi^{\boldsymbol{k}}_i$ and $\varepsilon^{\boldsymbol{k}}_i$ are eigenvectors and eigenvalues, $P^{\mu,\nu,\boldsymbol{g}}$ is an element of the density matrix, and $\chi^{\boldsymbol{0}}_{\mu}$ and $\chi^{\boldsymbol{g}}_{\nu}$ are atomic orbitals at the origin and in the $\boldsymbol{g}$-cells.

To summarize, in using the HF operator, the exchange part is calculated exactly and the correlation part is omitted, whereas in using the KS operator, the exchange and correlation parts are introduced into the Hamiltonian at different levels of approximation. The exchange/correlation potential is represented as a linear combination of gaussian-type functions and includes the translational periodicity of the crystal. Therefore, it is a basis of the total symmetric irreducible representation of the space group. In this work, the KS calculations lead to two levels of approximation:

(i) a local density approximation (LDA) scheme corresponding to the local exchange potential of Dirac [41] and the local correlation potential using the Perdew–Zunger [42] parametrization of Ceperley–Alder results [43];

(ii) a generalized gradient approximation (GGA) scheme corresponding to the use of non-local exchange and correlation potentials of Becke [44] and Perdew *et al* [45], respectively.

3. Methods of calculation of the Compton profiles and polarizabilities

3.1. Compton profiles

Within the impulse approximation in which the energy transfer to the recoil electrons must greatly exceed their binding energy, the directional Compton profile $J(p_z = q)$ is defined as the projection of the electron momentum density (EMD) $\rho(\boldsymbol{p})$ in the direction of the scattering vector:

$$J(q) = \int_{p_x p_y} \rho(\boldsymbol{p})\ \mathrm{d}p_x\ \mathrm{d}p_y. \tag{3}$$

In the momentum space, $\rho(\boldsymbol{p})$ is given by

$$\rho_{\mathrm{HF/KS}}(\boldsymbol{p}) = \sum_{\mu,\nu,\boldsymbol{g}} P^{\mu,\nu,\boldsymbol{g}}_{\mathrm{HF/KS}}\chi^{\boldsymbol{0}*}_{\mu}(\boldsymbol{p})\chi^{\boldsymbol{g}}_{\nu}(\boldsymbol{p}) \tag{4}$$

where $\chi^{\boldsymbol{0}}_{\mu}(\boldsymbol{p})$ and $\chi^{\boldsymbol{g}}_{\nu}(\boldsymbol{p})$ are the Fourier transformations of $\chi^{\boldsymbol{0}}_{\mu}(\boldsymbol{r})$ and $\chi^{\boldsymbol{g}}_{\nu}(\boldsymbol{r})$:

$$\chi(\boldsymbol{p}) = \int \chi(\boldsymbol{r})\mathrm{e}^{-\mathrm{i}\boldsymbol{p}\cdot\boldsymbol{r}}\ \mathrm{d}\boldsymbol{r}. \tag{5}$$

Finally, the directional Compton profile is expressed as

$$J_{\mathrm{HF/KS}}(q) = \sum_{\mu,\nu,\boldsymbol{g}} P^{\mu,\nu,\boldsymbol{g}}_{\mathrm{HF/KS}} \int_{p_x p_y} \chi^{\boldsymbol{0}*}_{\mu}(\boldsymbol{p})\chi^{\boldsymbol{g}}_{\nu}(\boldsymbol{p})\ \mathrm{d}p_x\ \mathrm{d}p_y \tag{6}$$

and the reciprocal form factor $B(z)$ is deduced by Fourier transformation of $J(q)$.

In order to obtain the average Compton profile, we first integrate the electronic density analytically:

$$\bar{\rho}_{\mathrm{HF/KS}}(\boldsymbol{p}) = \sum_{\mu,\nu,\boldsymbol{g}} P^{\mu,\nu,\boldsymbol{g}}_{\mathrm{HF/KS}} \frac{1}{4\pi} \int_{\theta=0}^{\pi} \int_{\varphi=0}^{2\pi} \chi^{\boldsymbol{0}*}_{\mu}(\boldsymbol{p}) \chi^{\boldsymbol{g}}_{\nu}(\boldsymbol{p}) \sin\theta \ \mathrm{d}\theta \ \mathrm{d}\varphi \tag{7}$$

over the spherical (θ, φ) coordinates corresponding to the p_z-direction. Then the average Compton profile is obtained numerically by means of the following integration:

$$\bar{J}(q) = \int_{p=q}^{\infty} \bar{\rho}(p) 2\pi p \ \mathrm{d}p. \tag{8}$$

3.2. Polarizability and related functions

The *polarizability* represents the linear response of the electric dipole of a system in an electric field. In the electric dipole Hamiltonian gauge, its dynamic expression which is explicitly given by the formulas 8.45 and 8.46 of reference [46] is written as

$$\alpha(\omega) = \sum_{n} f_n \left[\frac{\Delta E_n^2 - \omega^2}{(\Delta E_n^2 - \omega^2)^2 + \omega^2 \Gamma_n^2} + \frac{\mathrm{i}\Gamma_n \omega}{(\Delta E_n^2 - \omega^2)^2 + \omega^2 \Gamma_n^2} \right] \tag{9}$$

where f_n, ΔE_n and ω are oscillator strengths, transition energies and the electric field frequency, respectively, and $1/\Gamma_n$ corresponds to decay times introduced to represent the natural radiative relaxation of the levels and replaces the positive infinitesimal parameter η in the mathematical expression for the second-order scattering amplitude $\alpha(\omega)$ [47]. In the following, every Γ_n is equal to one small arbitrary Γ_1 value which leads to peak widths qualitatively comparable with those obtained for other cubic systems [48] and which avoids the poles problem (see also the Padé approximant method in reference [49]). In order to calculate this expression, equation (9), which generally converges slowly with the number of excited states (n), the uncoupled Hartree–Fock (UCHF) or uncoupled KS (UCKS) methods already described in reference [36] are used. In these methods, ΔE_n and f_n are given by

$$\Delta E_n = \varepsilon_j^{\boldsymbol{k}} - \varepsilon_i^{\boldsymbol{k}} \tag{10}$$

and

$$f_n = \frac{2}{3} (\varepsilon_j^{\boldsymbol{k}} - \varepsilon_i^{\boldsymbol{k}}) \langle \varphi_i^{\boldsymbol{k}} | \boldsymbol{r} | \varphi_j^{\boldsymbol{k}} \rangle \langle \varphi_j^{\boldsymbol{k}} | \boldsymbol{r} | \varphi_i^{\boldsymbol{k}} \rangle. \tag{11}$$

The sum over n in (9) is replaced by a sum over the occupied (i) and virtual (j) crystalline orbitals and over $\boldsymbol{k}$ with a geometrical weight $\Omega(\boldsymbol{k})$. The real part of the polarizability is therefore given by the following expression:

$$\alpha_{uv}(\omega) = \sum_{\boldsymbol{k}} \Omega(\boldsymbol{k}) \sum_{i,j} 2(\varepsilon_j^{\boldsymbol{k}} - \varepsilon_i^{\boldsymbol{k}}) \frac{\langle \varphi_i^{\boldsymbol{k}} | u | \varphi_j^{\boldsymbol{k}} \rangle \langle \varphi_j^{\boldsymbol{k}} | v | \varphi_i^{\boldsymbol{k}} \rangle}{(\varepsilon_j^{\boldsymbol{k}} - \varepsilon_i^{\boldsymbol{k}})^2 - \omega^2} \tag{12}$$

with $u, v = x$, y or z.

This relation is established from the following three approximations:

(i) the excited states n are monoexcitations from occupied $\varphi_i^{\boldsymbol{k}}$ to unoccupied $\varphi_j^{\boldsymbol{k}}$ crystalline orbitals at each k-point;

(ii) vertical transition energies between the ground state and the excited state are equal to the differences between eigenvalues, $\varepsilon_j^{\boldsymbol{k}} - \varepsilon_i^{\boldsymbol{k}}$, thus allowing us to neglect the exchange and Coulomb integrals;

(iii) interactions between monoexcitations by the unperturbed Hamiltonian are omitted ($\langle \varphi_{i'}^{\boldsymbol{k}'} \rightarrow \varphi_{j'}^{\boldsymbol{k}'} | \hat{H}_0 | \varphi_i^{\boldsymbol{k}} \rightarrow \varphi_j^{\boldsymbol{k}} \rangle = 0$).

These approximations allow us to obtain simple analytical formulas for the real and imaginary parts of the $\alpha(\omega)$ and without doing any integration over ω according to the Kramers–Krönig [30, 31, 46, 50] transformations.

Related functions such as the *dielectric constant* and *energy loss function* (ELF) can be deduced from $\alpha(\omega)$. For non-ionic systems like diamond and cBN, the frequency-dependent dielectric constant $\varepsilon(\omega)$ is related to the dynamic polarizability [30] by the relations

$$\frac{\varepsilon(\omega)-1}{\varepsilon(\omega)+2}=\frac{4\pi N}{3}\alpha(\omega) \qquad \varepsilon(\omega)=\left(1+\frac{8\pi N}{3}\alpha(\omega)\right)\Big/\left(1-\frac{4\pi N}{3}\alpha(\omega)\right) \tag{13}$$

where N is the number of atoms per unit volume. For these systems and for optical frequencies, the dielectric constant $\varepsilon(\omega)$ is equal to the optical one $\varepsilon_\infty(\omega)$ for which there is only an electronic contribution.

Moreover, the energy loss function, which is related to the interaction between an incident electron beam and the plasmon of the crystal [31, 33, 34], is obtained from $\varepsilon(\omega)$ via the relation

$$\mathrm{ELF}=-\mathrm{Im}\left[\frac{1}{\varepsilon(\omega)}\right]. \tag{14}$$

4. Results

Before reporting the calculations of the Compton profiles and polarizabilities of diamond and cBN, physical properties depending on the total energy have been calculated with the computational conditions described in section 2; these are given in table 1.

Table 1. The lattice parameter a (in Å), bulk modulus B (in GPa), binding energy BE (in Hartree), transverse optical frequencies ν_{TO} (in THz) and indirect and direct gaps ΔE (in eV) of the band structure calculated at the HF, LDA and GGA levels.

	Diamond				cBN			
	HF	LDA	GGA	Experiment*	HF	LDA	GGA	Experiment*
a	3.574[a]	3.560[b]	3.600[b]	3.560	3.619[a]	3.600[b]	3.640[b]	3.615
B	476[a]	447[b]	416[b]	443	416[a]	382[b]	360[b]	367
BE	0.396[a]	0.704[b]	0.561[b]	0.555	0.354[a]	0.609[b]	0.505[b]	0.498
ν_{TO}	44.6[a]	—	—	39.9	33.9[a]	—	—	31.6
ΔE_{ind}	12.1[a]	4.0[c]	4.0[c]	5.4[d]	13.5[a]	4.3[c]	4.4[c]	6.0[e]: 6.4[f]
ΔE_{dir}	13.8[a]	5.3[c]	5.6[c]	7.3[g]	18.9[a]	8.6[c]	8.8[c]	14.5[h]

* These experimental values of a, B, BE and ν_{TO} are given in reference [22].
[a] Reference [22].
[b] Reference [40].
[c] This work.
[d] Reference [51].
[e] Reference [60].
[f] Reference [61].
[g] Reference [59].
[h] Reference [62].

The results given in table 1 allow us to make the following comments.

(i) As is already known, the HF calculations overestimate the lattice parameter. The electron correlation effects are opposite according to the two models: the GGA leads to the

same conclusion as the HF calculations while the LDA underestimates (as expected) the lattice constant, except for diamond where the perfect agreement is fortuitous.

(ii) The bulk modulus (B) is overestimated as is the lattice parameter in the HF approximation while the correlation effect significantly improved the agreement of B with the experimental result.

(iii) The binding energy is well reproduced by the GGA and overestimated by the LDA whereas the HF method underestimates it because the correlation energy is entirely omitted.

(iv) DFT greatly reduces the gap with respect to HF theory with the same trend, whatever the exchange potential.

These results also show that the 6-21G* basis set with an additional d-like polarization function is of good quality since the calculated properties are fully in agreement with experiment. This conclusion is confirmed for the electronic structure of cBN from the comparison of calculated and experimental charge densities and structure factors [26].

Table 2. Average Compton profiles $J(q)$ calculated at the HF and KS (GGA) levels. q is the electron momentum (in au).

	C (diamond)			cBN		
q	HF	KS (GGA)	Experiment[a]	HF	KS (GGA)	Experiment[b]
0.0	4.30	4.31	4.17	4.25	4.26	4.08 ± 0.08
0.1	4.28	4.29	4.17	4.23	4.24	4.05
0.2	4.23	4.23	4.11	4.18	4.19	4.00
0.3	4.13	4.14	4.01	4.09	4.10	3.98
0.4	4.01	4.01	3.88	3.96	3.98	3.91
0.5	3.85	3.85	3.75	3.80	3.81	3.70
0.6	3.65	3.66	3.57	3.61	3.62	3.50
0.7	3.43	3.43	3.35	3.38	3.38	3.24
0.8	3.17	3.17	3.10	3.12	3.12	2.93
0.9	2.88	2.88	2.86	2.84	2.84	2.64
1.0	2.57	2.57	2.58	2.54	2.53	2.39 ± 0.05
1.2	1.90	1.88	1.88	1.89	1.87	1.86
1.4	1.27	1.25	1.33	1.31	1.28	1.45
1.6	0.87	0.86	0.90	0.92	0.91	1.13
1.8	0.66	0.67	0.72	0.71	0.71	0.86
2.0	0.56	0.57	0.62	0.59	0.60	0.68 ± 0.02
2.5	0.41	0.42	0.46	0.43	0.43	0.45
3.0	0.32	0.32	0.35	0.32	0.32	0.35
4.0	0.19	0.19	0.21	0.19	0.19	
5.0	0.11	0.11	0.12	0.11	0.11	
8.0	0.02	0.02	0.02	0.02	0.02	

[a] Reference [5].
[b] Reference [6].

4.1. Compton profiles

The average and directional Compton profiles (CPs) and the anisotropy of the Compton profiles calculated at the HF and KS levels are given in tables 2 and 3, and figure 1, respectively. All of the CPs are normalized to 12, which represents the number of electrons in the unit cell. Experimental average CPs are also given for comparison. Not all of the values are reported, for reasons of clarity:

Table 3. Directional Compton profiles $J(q)$ calculated at the KS (GGA) level. q is the electron momentum (in au).

	C (diamond)			cBN		
q	[100]	[110]	[111]	[100]	[110]	[111]
0.0	4.34	4.39	4.18	4.27	4.30	4.19
0.1	4.33	4.37	4.16	4.26	4.28	4.18
0.2	4.28	4.30	4.12	4.22	4.23	4.13
0.3	4.20	4.16	4.07	4.15	4.12	4.06
0.4	4.08	3.97	4.00	4.04	3.97	3.96
0.5	3.93	3.78	3.89	3.89	3.78	3.82
0.6	3.72	3.57	3.73	3.68	3.55	3.65
0.7	3.45	3.33	3.53	3.41	3.29	3.44
0.8	3.13	3.07	3.27	3.10	3.04	3.18
0.9	2.79	2.84	2.96	2.77	2.83	2.88
1.0	2.43	2.62	2.60	2.43	2.60	2.54
1.1	2.09	2.36	2.23	2.09	2.31	2.20
1.2	1.77	2.01	1.88	1.78	1.97	1.88
1.3	1.48	1.61	1.56	1.50	1.61	1.58
1.4	1.24	1.26	1.29	1.27	1.29	1.33
1.5	1.04	0.99	1.06	1.08	1.05	1.11
1.6	0.89	0.83	0.89	0.94	0.88	0.94
1.7	0.78	0.72	0.76	0.83	0.76	0.81
1.8	0.70	0.65	0.66	0.74	0.69	0.71
1.9	0.64	0.60	0.60	0.68	0.63	0.64
2.0	0.59	0.56	0.54	0.62	0.59	0.58
2.5	0.43	0.43	0.40	0.44	0.45	0.42
3.0	0.32	0.33	0.33	0.33	0.33	0.33
4.0	0.19	0.19	0.19	0.19	0.19	0.19
5.0	0.11	0.11	0.11	0.11	0.11	0.11
8.0	0.02	0.02	0.02	0.02	0.02	0.02

(i) the KS values obtained at the LDA and GGA levels are identical;

(ii) the difference between the HF and KS values (table 2) is very small and not significant. This result is confirmed with the directional CPs and, therefore, the values are reported only for the KS (GGA) model.

The basis set effect must be underlined because it also determines the accuracy of the calculations. In the case of cBN, the 7-311G* basis set already documented in the hBN study [38] was used after accommodation to the experimental cubic geometry. It leads to directional CP values very close to those obtained with the 6-21G* set, making the CP anisotropies $J_{100} - J_{111}$ and $J_{100} - J_{110}$ higher by 0.005 and 0.01 au than those calculated with the 6-21G* set in the valence region ($q < 0.4$ au). This effect is very small as for hBN and shows that the quality of the 6-21G* basis set is satisfactory in order to compare the EMD of diamond and cBN.

4.1.1. Comparison with experiment and other calculations. To our knowledge, the experimental data for CPs are not numerous and are twenty five years old for the more recently discovered ones. For diamond, average and directional CPs have been measured by Weiss and Phillips [4] and by Reed and Eisenberger [5] using x-rays and 160 keV γ-rays, respectively. Only these latter more accurate CPs are reported in table 2 and figure 1 for comparison. For cBN, the data of Weiss [6] obtained from measurements on polycrystalline

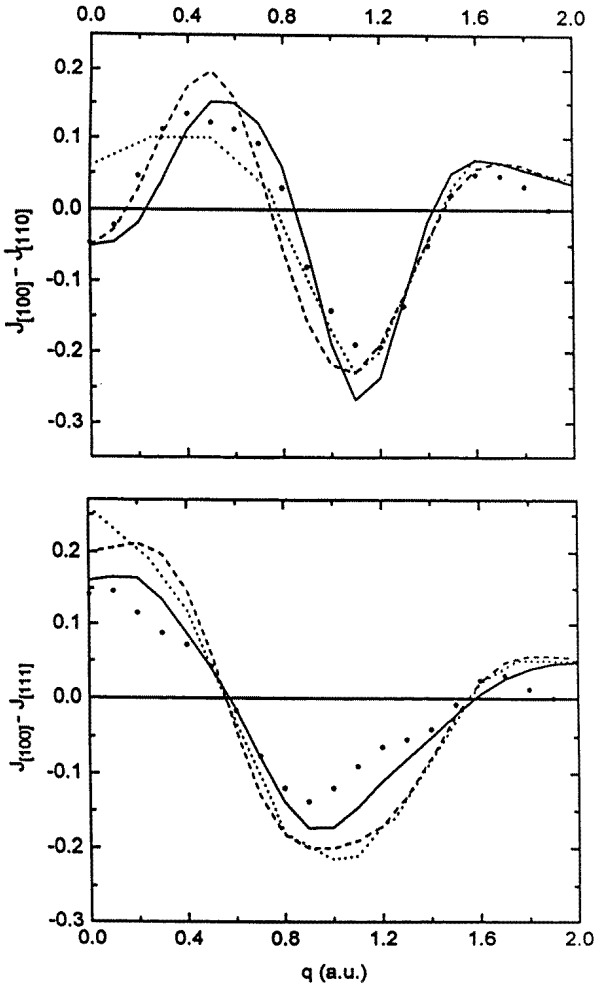

(a)

Figure 1. The Compton profile anisotropies $J_{100} - J_{110}$ and $J_{100} - J_{111}$ of diamond (a) and of cBN (b). Full and dotted lines correspond to our present calculations and to those of Dovesi *et al* [21] performed using a minimal STO-3G basis set, respectively. Dashed lines correspond to the SCF-HF calculations of Euwema *et al* [11, 19]. Circles (a) represent the experimental results of Reed and Eisenberger [5].

samples are available. As in all cases, the theoretical CPs are larger than the experimental ones. This observation is confirmed by the SCF-HF calculations of Wepfer *et al* [11], of Seth and Ellis [12] and of Dovesi *et al* [21], and by the model of a one-electron density matrix containing only interactions between nearest neighbours developed by Schülke and Kramer [14] for diamond, and by the SCF-HF calculations of Euwema *et al* [19] and of Dovesi *et al* [21] for cBN. Generally speaking, the agreement between our calculations and experiment is highly satisfactory. It is better for diamond than for cBN, and for the directional CPs than for the average CPs.

Figure 1(a) shows that the best agreement between theory and experiment is obtained with our calculations. However, the $J_{100} - J_{110}$ anisotropy is reproduced better in the region

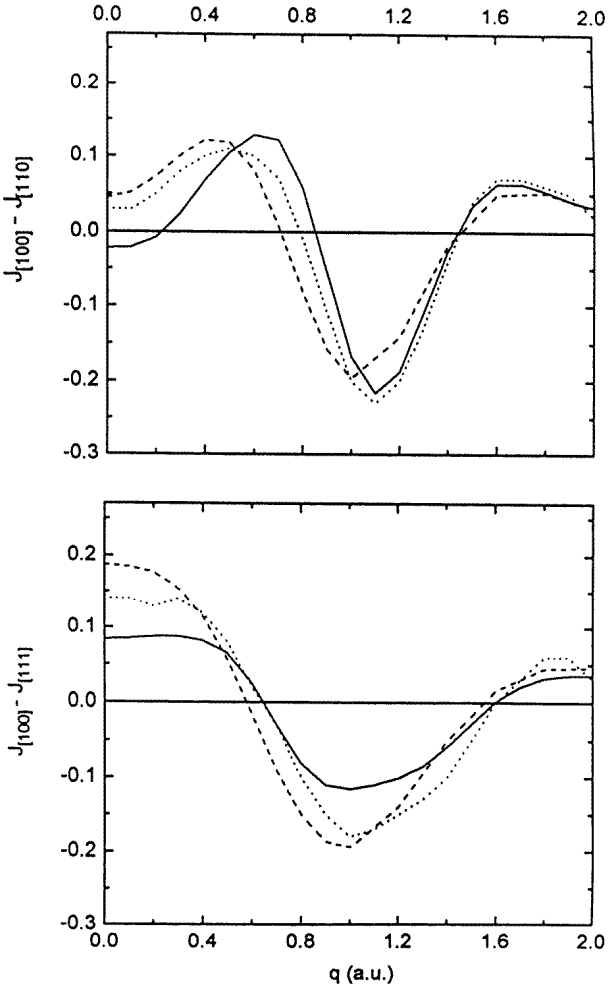

(b)

Figure 1. (Continued)

of the smallest values of the momentum by the calculations of Wepfer *et al* [11] or of Seth and Ellis [12], but this improvement remains confined to this region only. The comparison between our calculations and those of Dovesi *et al* [21] carried out with the same method is very instructive because it shows the improvement of CRYSTAL during these fifteen years. The use of more severe tolerances, the use of more k-points in the irreducible part of the first Brillouin zone and above all the possibility of using more extended basis sets (6-21G* instead of STO-3G) explains why the improvement of the calculations is significant for diamond, large for cBN (figure 1(b)) and can be considerable for hBN where the STO-3G set leads to poor results [38]. With these conclusions and taking into account the closeness of the calculations of Euwema *et al* [19] and of Dovesi *et al* [21] and the absence of experimental data, it can be concluded, as for diamond, that our CP anisotropies of cBN are more reliable. In particular, the $J_{100} - J_{110}$ anisotropy becomes similar to that of diamond since it presents a negative part in the region of the smallest values of the momentum.

Several reasons can be invoked to explain why the theoretical CPs are more peaked at low momenta than the experimental data.

(i) Our theoretical results are not convolved since the authors do not give the values of the residual instrumental function (RIF): in these conditions, the difference is pessimistic since, for example, taking RIF $= 0.15$ au [14] decreases the theoretical value of J by about 0.5%.

(ii) From a theoretical point of view, two important factors must be considered to explain the remaining difference. The first one is associated with the quality of the basis set (figure 1(a)). The second one concerns the correlation effect of which the true value cannot be deduced from the comparison of HF and (standard) KS calculations. Within DFT, general ground-state expectation values (like that of the electron momentum density) can only be determined formally correctly by the inclusion of a correction term (not done in this work) which would then lead to a noticeable difference between the CPs at the HF and (correlation-corrected) KS levels. However, electron correlation in the ground state is an important aspect in Compton scattering which is still awaiting a definitive theoretical treatment.

(iii) Finally, it can be noted that using C or cBN single crystals in place of diamond dust [5] or the cBN polycrystalline sample [6] should contribute to improving the agreement.

4.1.2. Conclusions. Homogeneous calculations of CPs have been presented. They lead to a better agreement with experiment than the other SCF-HF calculations mentioned. The CP anisotropy curves are similar for diamond and cBN. This result is not surprising since the two compounds are isoelectronic, and they have the same structure with close lattice parameters and slightly different space-group symmetries. However, the magnitude of the $J_{100} - J_{111}$ anisotropy is higher for diamond than for cBN and must be correlated with the different characters of the chemical bonds. Finally, we note that an excellent agreement has recently been obtained between our calculations and experiment for hBN [38]. For diamond and cBN the agreement is less good but it could be improved with new experiments taking advantage of the technical progress and reporting measured total CPs without separating the valence part from the core, which can induce additional errors when the core is deformed by the crystal-field effect.

4.2. Polarizability and related functions

4.2.1. Static polarizability and the dielectric constant. The static polarizability values per unit cell obtained from expression (12) with $\omega = 0$ are given in table 4 for diamond and cBN at both the HF and KS (GGA) levels of calculation. KS crystalline orbitals at the LDA and GGA levels lead, as for CPs, to similar polarizability values (1.66 Å^3 for diamond, 1.32 Å^3 for cBN). Moreover they are in good agreement with the other results: 1.64 Å^3 [51] and 1.51 Å^3 [32] for diamond and cBN respectively, while the HF values are too small (1.04 Å^3 for diamond, 0.78 Å^3 for cBN). To understand this difference, it is necessary to consider the numerator and denominator contributions to the polarizability calculation separately.

(i) The denominator in (12) is related to the direct gap which is the smallest ε_i^k to ε_j^k vertical transition, obtained at the Γ point for diamond and cBN (table 1). With the HF method, this gap is systematically overestimated as mentioned by Orlando *et al* [22] (for diamond, the factor is 2), while the KS method underestimates it less. This trend is general for DFT calculations [50, 52, 53] and is due to the fact that the DFT exchange potentials do not contain exchange singularity [54].

Table 4. The static polarizability α (Å^3) per unit cell, dielectric constant (ε) and plasmon energy E_p (eV) calculated at the HF and KS (GGA) levels for diamond and cBN.

	Diamond			cBN		
	HF	GGA	Others	HF	GGA	Others
$\sum_n f_n$	13.14	8.97		11.64	8.16	
α	1.04	1.66	1.64*	0.78	1.32	1.51*
ε	2.89	5.86	5.7[a]	2.16	3.63	4.46[b]
E_p	52.3	36.4	33.6[c] 33.3[e] 32.0[d]	50.3	35.4	29.0[d] 30.4[f]

* Obtained from ε by means of equation (13).
[a] Reference [51].
[b] Reference [32].
[c] Reference [63].
[d] Reference [34].
[e] Reference [64].
[f] Reference [33].

(ii) The values of the sum ($\sum_n f_n$) over the oscillator strengths (the numerator of (12)) which must be the values of the number n_e of electrons per cell are underestimated when calculated at the KS level (8.98 and 8.16 for diamond and cBN respectively instead of 12). In contrast, they are close to the theoretical values obtained using the HF method (13.14 and 11.64). Therefore, if UCKS calculations of the static polarizability lead to a better agreement with experiment, this results from a balance of the errors associated with the evaluation of the numerator and the denominator of equation (12). At the HF level, the calculated α-values are too small even if the oscillator strengths f_n obey the Thomas–Reiche–Kuhn formula $\sum_n f_n = n_e$ within an error bar smaller than 10%; this is due to the overestimation of the gap value. A scissors operator method which consists in shifting the calculated gap (see reference [48] for example) in order to obtain the experimental one can be applied to improve the UCHF results. This leads to $\alpha = 1.38$ Å^3 for diamond [36] and 0.93 Å^3 for cBN (1.04 Å^3 and 0.78 Å^3 respectively without correction), which is still too small compared to the UCKS and experimental values (table 4).

Our static dielectric constant ε-values are deduced from the calculated polarizabilities by means of the Clausius–Mossotti relation (13). They are reported in table 4. A better agreement with experiment is obtained when they are calculated at the KS level for the reasons previously indicated for the polarizability.

4.2.2. The dynamic dielectric constant. In order to calculate optical properties of solids, which can be obtained from reflectance measurements, the electric field frequency has to be taken into account. Equations (9), (10) and (11) allow us to calculate the dynamic polarizability and to deduce the optical dielectric constant. In figure 2, the variations of the real (ε_R) and imaginary (ε_I) parts of the dielectric constant of diamond and cBN, calculated at the KS level, are plotted in the range $\hbar\omega = 0$–15 eV and for a decay time $1/\Gamma_1$ equal to 200 au. This Γ_1 value (0.005) has also been used by Eremets *et al* [32] to simulate the dispersion of the refractive index of cBN.

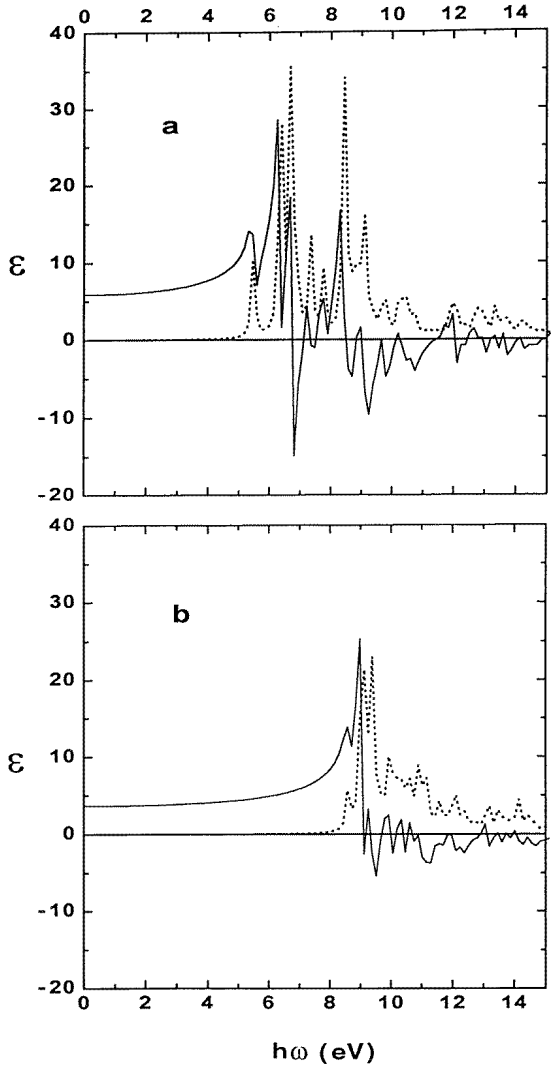

Figure 2. The real (full lines) and imaginary (dotted lines) parts of the dielectric constant calculated at the KS (GGA) level for diamond (a) and cBN (b).

The first lower-energy peak of the $\varepsilon_R(\omega)$ spectra appears at such an ω-value that the real part of the atomic polarizability is equal to $3/(4\pi N)$ according to equation (13) (this is the condition for a polarization catastrophe [31]); the $\alpha_R(\omega)$ values per unit cell deduced are 2.69 Å^3 and 2.82 Å^3 for diamond and cBN respectively. The corresponding energy value $\overline{h}\omega$ is close to the direct gap (5.5 and 8.7 eV for diamond and cBN respectively) since $\alpha_R(\omega)$ remains practically constant below the first resonance and only begins to increase rapidly near to it. The $\varepsilon_I(\omega)$ spectrum is also related to the polarizability and to the scattering cross-section. As for $\varepsilon_R(\omega)$, the first peaks appear at energy values close to the gap, then at lower frequencies for diamond. But it is interesting to notice that the diamond spectrum is much more spread out than that of cBN. This is why the static polarizabilities or dielectric constants of diamond and cBN are close, even if the cBN gap is twice that of diamond.

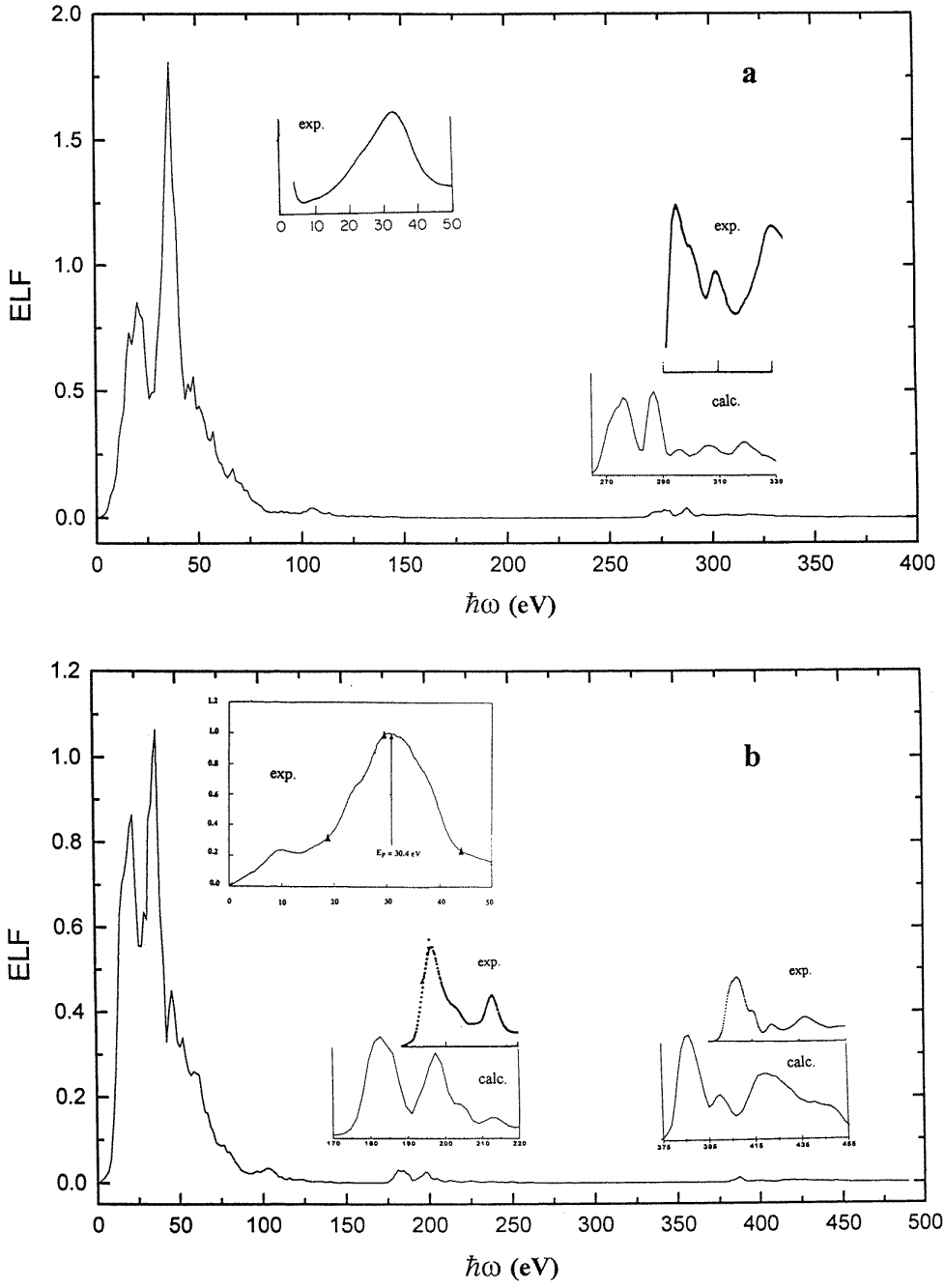

Figure 3. The energy loss function at the KS (GGA) level versus the energy of an incident electron beam (in eV) for diamond (a) and cBN (b). The insets give the calculated (calc.) and experimental (exp.) spectra corresponding to the interesting energy ranges (the experimental ones come from reference [34] for diamond and reference [33] for cBN).

4.2.3. The energy loss function (ELF). In figure 3, the energy loss function deduced from the dynamic dielectric constant (equation (14)) calculated at the KS level has been plotted for diamond and cBN. For both compounds, a broad band including two high peaks appears in the low-energy range. The highest peak, which leads to the plasmon energy $E_p = 36.4$ eV for diamond and 35.4 eV for cBN, was observed by Hosoi *et al* [34] at 29 eV and 32 eV, respectively. Other experimental values are given in table 4. It follows that these σ-plasmon energies obtained at the KS level are slightly too large compared with the experimental ones, while the unreported HF values are worse. The narrow bands observed at larger frequencies are due to core-electron excitations. The corresponding energies are 182 eV (B) and 386 eV (N) for cBN, and 277 eV for diamond. They can be compared with the experimental values: 195 eV [33, 34] for B, 405 eV [34] and 409 eV [33] for N, and 291 eV [34] and 294 eV [35] for C, from the spectra of the K edge of the cBN and diamond compounds. Our energy values obtained at the KS level are smaller than the experimental ones whereas the HF values are still much too large. It is interesting to notice that the B and C bands given in figure 3 for cBN and diamond show in fact a second peak at 16 eV and 11 eV above the first one, respectively. This peak was also observed at 18 eV for both compounds by Gonnet [33] and at 12 eV by Egerton and Whelan [35] for diamond. It seems to be a typical feature of the zinc-blende structure, as also mentioned by McKenzie *et al* [55]. The experimental data reported in figure 3 show ELF behaviour similar to what we found, in spite of slight energy shifts.

5. Discussion and concluding remarks

New first-principles calculations of the crystalline wave function of diamond and cBN described with a 6-21G* all-electron basis set have been presented for the LCAO DFT method with a very good degree of accuracy thanks to the recent improvements introduced into the CRYSTAL program. The ground-state electronic structure deduced from average and directional CPs and the polarizability and its related functions have been reported. Compared to the HF results, the part of the correlation effect taken into account in the LCAO-DFT calculation can be very different according to whether just the ground-state property, namely the Compton profile, or the polarizability related also to the excited states is taken into consideration. For the Compton profile and its related functions (the electron momentum density and reciprocal form factor), this effect is small, while it greatly modifies the polarizability values and related functions via the gap value.

Nowadays, the ground-state electronic structures of diamond and cBN are well known from theoretical and experimental studies of x-ray scattering factors, the charge density and directional CPs. In the case of diamond, the studies of Takama *et al* [3], Zunger and Freeman [13], Pattison *et al* [16], Spackman [17] and Lu *et al* [18], interpreting the data of Reed and Eisenberger [5] and of Seth and Ellis [12], are considered as definitive. In the same way, we will quote the papers of Will *et al* [7], Eichhorn *et al* [8], Zunger and Freeman [20], Xu and Ching [23], Bross and Bader [25] and Lichanot *et al* [26] for cBN. From these investigations, the main differences between the two electronic distributions can be summarized as follows: the bonding between two nearest-neighbour atoms is symmetric in diamond (purely covalent bonds) and non-symmetric in cBN where there is an electron charge transfer from boron to nitrogen (semi-covalent bonds). More precisely:

(i) in diamond, a monotonic decrease of the total charge density from the atomic positions to the point midway between the two atoms [22] is observed, whereas in silicon, for example, there is a large plateau of nearly constant density; this makes the bond charge

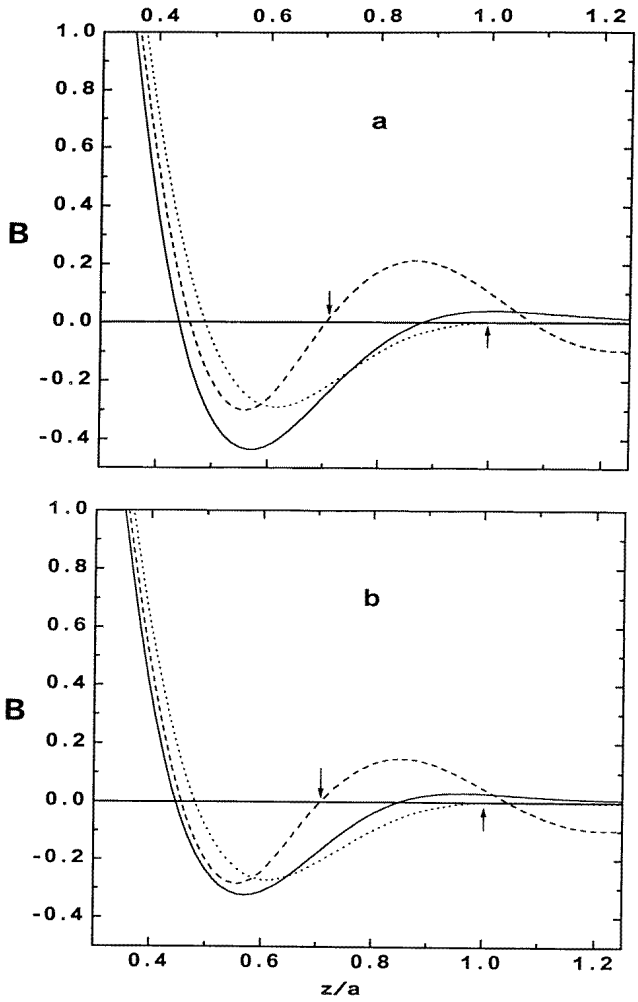

Figure 4. Directional reciprocal form factors $B(z)$. The dotted, dashed and full lines are associated with the [100], [110] and [111] directions, respectively. The abscissa gives the normalized distance z/a where a is the lattice parameter. (a) Diamond. (b) cBN. The arrows indicate the reference values of z/a ($1/\sqrt{2}$ and 1) along the [110] and [100] directions.

of silicon much more diffuse than that of diamond where the lack of core p electrons allows the valence electrons to get nearer to the nuclei;

(ii) in cBN, the charge transfer from B to N localizes the bond charge nearer to the nitrogen but close to the midpoint between B and N [26], and the charge-density maximum of cBN is only slightly lower than that of diamond.

Examination of table 2 reveals that the CP values of diamond and cBN are close, but slightly higher for diamond than for cBN in the region of small values of the momentum ($q < 1$ au). This result is confirmed when the directional CPs are examined except for the [111] direction of the chemical bond at the smallest q-values ($q < 0.3$ au) (see table 3). In consequence, the 'long-range' $J_{100} - J_{110}$ anisotropies are practically identical for the two compounds whereas the $J_{100} - J_{111}$ anisotropy, which involves the bond direction, is for

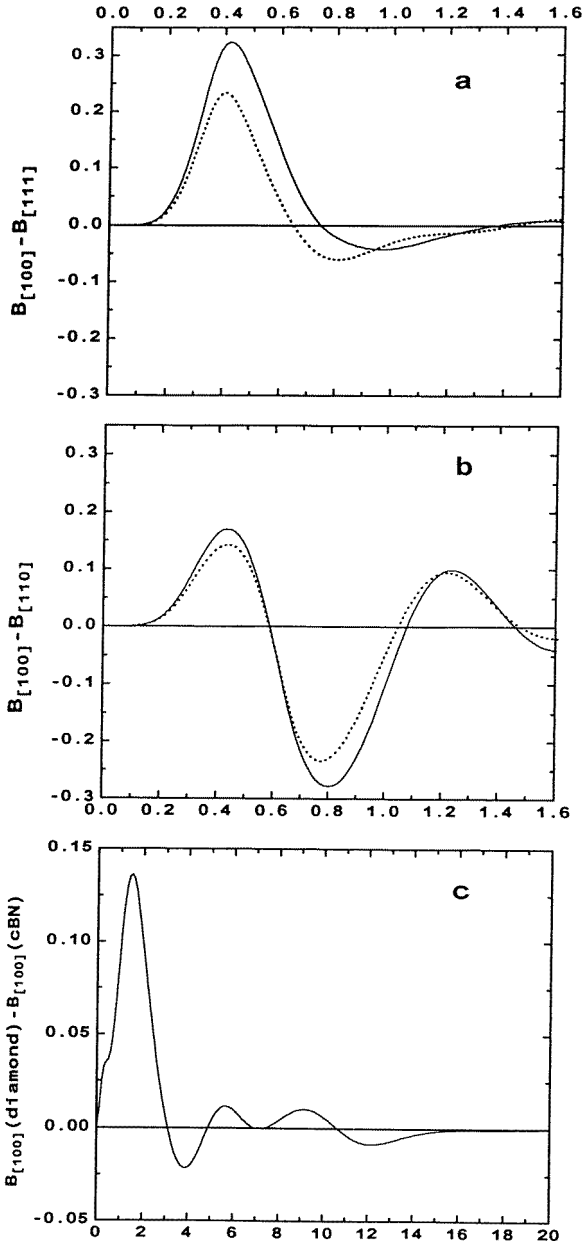

Figure 5. The reciprocal-form-factor anisotropy versus the normalized distance z/a. The full and dotted lines are for diamond and cBN, respectively. (a) $B_{100} - B_{111}$ anisotropy; (b) $B_{100} - B_{110}$ anisotropy; (c) B_{100}(diamond) $- B_{100}$(cBN) versus z (in au).

cBN half that for diamond. This result confirms the conclusions drawn for the direct space from the studies of the charge density $\rho(\boldsymbol{r})$.

In order to facilitate the identification of bonding features in the direct space, a reciprocal form factor or autocorrelation function $B(\boldsymbol{r})$ is introduced as the Fourier transformation

of the Compton profile. By using a 1D Fourier transform, $B(z) = \int J(p_z)\mathrm{e}^{-\mathrm{i}p_z z}\,\mathrm{d}p_z$ is calculated along the three crystallographic axes and the $B_{100}(z)$, $B_{110}(z)$ and $B_{111}(z)$ values are reported in figure 4 versus the normalized distance z/a. Diamond and cBN are semiconductors with filled bands and, for such crystals, $B(z)$ should have a zero value at all lattice translational vector points due to the long-range AO overlap of the neighbour unit cells [56]. In all cases, our theoretical curves (figure 4) cross the z/a axis at the appropriate values, providing a check on the accuracy and reliability of the wave functions. The negative parts of $B(z)$ are attributable to the effects of antibonding interactions arising from the second-nearest-neighbour overlap. Figure 4 shows that these effects are similar in diamond and cBN and take place up to 4 Å. However, the largest difference between the diamond and cBN is given by the $B_{111}(z)$ curves which exhibit a significantly stronger anisotropy in the diamond case. In order to illustrate and compare the anisotropies of the chemical bonds in diamond and cBN, the treatment by Pattison *et al* [16] of diamond is adopted here. The differences $B_{100} - B_{111}$ and $B_{100} - B_{110}$ should reveal the strongest effects of the bond anisotropy and antibonding interactions, respectively, if the [100] direction acts as a neutral direction. This assumption is valid for both compounds since no special feature is observed in the B_{100}(diamond)–B_{100}(cBN) curve (figure 5(c)) which is close to zero when z is greater than 3 au. For both compounds, the B-anisotropy shows prominent features at the nearest first- and second-neighbour distances. At the bond length ($z/a = \sqrt{3}/4$), the $B_{100} - B_{111}$ curve indicates that the bond anisotropy is stronger for diamond than for cBN. The $B_{100} - B_{110}$ curves which are close for the two compounds are dominated by a non-bonding interaction between the orbitals which form neighbouring bonds in the lattice. It takes place at a distance of $z/a = 1/\sqrt{2}$ between second-nearest neighbours and it results from the diffuse character of the bond charge shown in the ECHD maps [22]. Finally, the electron momentum density and related properties of diamond and cBN are rather close, the only difference being the stronger bond anisotropy in diamond. This result seems attributable simply to the different characters of the bonds, namely that the sp^3 orbitals are more localized near to the N nuclei because of the charge transfer between B and N. In fact, the comparison of CPs for the two compounds is rather easy because it removes the geometry and valence electron configuration effects, since the lattice parameters are very close and the valence electrons belong to the same shell. These two factors are decisive in underlining the main differences between the $B(z)$ anisotropies in diamond and silicon, which are dominated in this latter compound by the 'long-range' orbital overlap [16, 56].

For the polarizability property, which in addition depends on the description of the excited states, the calculations for diamond and cBN crystals found in the literature are not numerous, unlike the case for experimental results on related functions like the dielectric constant and the energy loss function. Effectively, the calculations are strongly gap dependent for these semiconductors and the electronic correlation cannot be neglected. Since the perturbation theory of the electronic correlation in periodic systems is not available, as in the study of infinite polyenes by Suhai [57], the DFT approximation has been used to partly take this into account. Using our uncoupled method with the KS crystalline orbitals, the polarizability values obtained for diamond and cBN are relatively close to the experimental ones.

Moreover, cBN and diamond have spectral similarities not only in the plasmon loss spectra but also in the core-edge spectra (as also mentioned by Hosoi *et al* [34]), the sole significant difference being as regards the energy positions of the core-electron excitations. It is noted that the difference between silicon and diamond, though they belong to the same chemical family, is larger than that between diamond and cBN as regards the polarizability, dielectric constant and plasmon energy ($\varepsilon = 8.4$ and $E_p = 20$ eV from our DFT calculations

for Si [36]). This is probably due to the small gap of Si, with a narrow ε-spectrum. However, our results concerning the core-edge spectra must be moderated by the following remark: the electric dipole approximation no longer holds for the range of energy in which these peaks appear and the behaviour of the core-edge spectra could be slightly modified [58].

6. General conclusions

In this work, the Compton profiles and polarizability and their related functions for diamond and cBN have been studied at two levels of calculation, according to the LCAO-HF and LCAO-DFT methods used. Compton profiles and reciprocal form factors, which depend on the electron momentum densities, need only the knowledge of the ground state. However, only a part of the electronic correlation effect is taken into account with the LCAO-DFT method: for these properties, it is small for both compounds. The polarizability and related functions (the dielectric constant and energy loss function) are gap dependent and are much more sensitive to the electron correlation effect. In fact, the HF or KS methods used to calculate them lead to overestimation and underestimation, respectively. Better results are obtained with DFT.

Because of their similar electronic and geometric structures, diamond and cBN have similar Compton profiles. However, the semi-covalent character of cBN is revealed by the smaller anisotropy of the reciprocal form factors relating to the bond direction. In contrast, different values of the polarizabilities of diamond and cBN were expected because cBN has a direct gap twice as large as the diamond one with the same theoretical value ($n_e = 12$) of the sum of the oscillator strengths; but in fact, the polarizability values are close, showing the importance of the band widths of the $\varepsilon(\omega)$ spectra.

Finally, Compton profiles, the polarizability and their related properties are complementary probes allowing one to observe small differences between the electronic structures of similar compounds. However, progress must be made in describing the excited states of solids.

References

[1] Wentorf R H 1957 *J. Chem. Phys.* **26** 956
Wentorf R H 1961 *J. Chem. Phys.* **34** 809
[2] Göttlicher S and Wölfel E 1959 *Z. Elektrochem.* **63** 891
[3] Takama T, Tsuchiya K, Kobayashi K and Sato S 1990 *Acta Crystallogr.* A **46** 514
[4] Weiss R J and Phillips W C 1968 *Phys. Rev.* **176** 900
[5] Reed W A and Eisenberger P 1972 *Phys. Rev.* B **6** 4596
[6] Weiss R J 1974 *Phil. Mag.* **29** 1029
[7] Will G, Kirfel A and Josten B 1986 *J. Less-Common Met.* **117** 61
[8] Eichhorn K, Kirfel A, Grochowski J and Suda P 1991 *Acta Crystallogr.* B **47** 843
[9] Lopatin V V and Konusov F V 1992 *J. Phys. Chem. Solids* **53** 847
[10] Euwema R N, Wilhite D L and Surratt G T 1973 *Phys. Rev.* B **7** 818
[11] Wepfer G G, Euwema R N, Surratt G T and Wilhite D L 1974 *Phys. Rev.* B **9** 2670
[12] Seth A and Ellis D E 1977 *J. Phys. C: Solid State Phys.* **10** 181
[13] Zunger A and Freeman A J 1977 *Phys. Rev.* B **15** 5049
[14] Schülke W and Kramer B 1979 *Acta Crystallogr.* A **35** 953
[15] Dovesi R, Pisani C, Ricca F and Roetti C 1980 *Phys. Rev.* B **22** 5936
[16] Pattison P, Hansen N K and Schneider J R 1981 *Chem. Phys.* **59** 231
[17] Spackman M A 1991 *Acta Crystallogr.* A **47** 420
[18] Lu Z W, Zunger A and Deutsch M 1993 *Phys. Rev.* B **47** 9385
[19] Euwema R N, Surratt G T, Wilhite D L and Wepfer G G 1974 *Phil. Mag.* **29** 1033
[20] Zunger A and Freeman A J 1978 *Phys. Rev.* B **17** 2030

[21] Dovesi R, Pisani C, Roetti C and Dellarole P 1981 *Phys. Rev.* B **24** 4170
[22] Orlando R, Dovesi R, Roetti C and Saunders V R 1990 *J. Phys.: Condens. Matter* **2** 7769
[23] Xu Y N and Ching W Y 1991 *Phys. Rev.* B **44** 7787
[24] Furthmüller J, Hafner J and Kresse G 1994 *Phys. Rev.* B **50** 15 606
[25] Bross H and Bader R 1995 *Phys. Status Solidi* b **191** 369
[26] Lichanot A, Azavant P and Pietch U 1996 *Acta Crystallogr.* B **52** 586
[27] Pisani C, Dovesi R and Roetti C 1988 *Hartree–Fock ab initio Treatment of Crystalline Systems (Springer Lecture Notes in Chemistry 48)* (Heidelberg: Springer)
[28] Dovesi R, Pisani C, Roetti C, Causà M and Saunders V R 1988 *CRYSTAL 88* Program No 577, Quantum Chemistry Program Exchange, Indiana University, Bloomington, IN
[29] Dovesi R, Saunders V R, Roetti C, Causà M, Harrison N M, Orlando R and Aprà E 1995 *CRYSTAL 95* Users Manual, Theoretical Chemistry Group (Turin) and CCLRC Daresbury Laboratory (Didcot, UK)
[30] Ashcroft N W and Mermin N D 1976 *Solid State Physics* (New York: Holt, Rinehart and Winston)
[31] Kittel C 1976 *Physique de l'État Solide* Dunod University edn (Chichester: Wiley)
[32] Eremets M I, Gauthier M, Polian A, Chervin J C, Besson J M, Dubitskii G A and Semenova Ye Ye 1995 *Phys. Rev.* B **52** 8854
[33] Gonnet V 1994 *Thesis* University of Bordeaux I (No 1199)
[34] Hosoi J, Oikawa T, Inoue M, Matsui Y and Endo T 1982 *J. Electron Spectrosc. Relat. Phenom.* **27** 243
[35] Egerton R F and Whelan M J 1974 *J. Electron Spectrosc. Relat. Phenom.* **3** 232
[36] Ayma D, Campillo J P, Rérat M and Causà M 1997 *J. Comput. Chem.* **18** 1253
[37] Dovesi R, Saunders V R and Roetti C 1992 *CRYSTAL 92* Users Manual, Università di Torino
[38] Lichanot A, Rérat M and Causà M 1996 *J. Phys.: Condens. Matter* **8** 10 425
[39] Causà M and Zupan A 1994 *Quantum Chem. Symp.; Int. J. Quantum Chem.* **28** 633
[40] Zupan A and Causà M 1995 *Int. J. Quantum Chem.* **56** 337
[41] Dirac P A M 1930 *Proc. Camb. Phil. Soc.* **26** 376
[42] Perdew J P and Zunger A 1981 *Phys. Rev.* B **23** 5048
[43] Ceperley D M and Alder B J 1980 *Phys. Rev. Lett.* **45** 566
[44] Becke A 1988 *Phys. Rev.* A **88** 1053
[45] Perdew J P and Wang Y 1991 *Phys. Rev.* B **45** 13 244
Perdew J P, Chevary J A, Vosko S H, Perderson M R, Singh D J and Fiolhais C 1992 *Phys. Rev* B **46** 6671
[46] Ziman J M 1969 *Principles of the Theory of Solids* (Cambridge: Cambridge University Press)
[47] Cohen-Tannoudji C, Dupont-Roc J and Grynberg G 1988 *Processus d'Interaction Entre Photons et Atomes* (Paris: InterEditions)
[48] Ching W Y, Gan F and Huang M Z 1995 *Phys. Rev.* B **52** 1596
[49] Lee K H and Chang K J 1996 *Phys. Rev.* B **54** 8285
[50] Mo S D and Ching W Y 1995 *Phys. Rev.* B **51** 13 023
[51] *CRC Handbook of Chemistry and Physics* 1988–1989 69th edn, ed R C Weast (Cleveland, OH: Chemical Rubber Company Press)
Phillips J C 1968 *Phys. Rev. Lett.* **20** 550
[52] Svane A and Andersen D K 1986 *Phys. Rev.* B **34** 5512
[53] Froyen S and Cohen M L 1984 *Phys. Rev.* B **29** 3770
Froyen S and Cohen M L 1986 *J. Phys. C: Solid State Phys.* **19** 2623
[54] Assing G and Monkhorst H J 1993 *Int. J. Quantum Chem. Symp.* **27** 81
[55] McKenzie D R, Cockayne D J H, Muller D A, Murakawa M, Miyake S, Watanabe S and Fallon P 1991 *J. Appl. Phys.* **70** 3007
[56] Williams B G and Thomas J M 1983 Compton scattering as a technique for the study of solids *International Reviews in Physical Chemistry* vol 39 (Oxford: Butterworth)
[57] Suhai S 1992 *Int. J. Quantum Chem.* **42** 193
[58] Forsyth A J, Josefsson T W and Smith A E 1996 *Phys. Rev.* **54** 14 355
[59] Godby R W, Schluter M and Sham L J 1987 *Phys. Rev.* **36** 6497
[60] Formichev V A and Rumsh M A 1968 *J. Phys. Chem. Solids* **29** 1015
[61] Chrenko R M 1968 *Solid State Commun.* **14** 511
[62] Phillip H R and Taft E A 1962 *Phys. Rev.* B **127** 159
[63] Wang Y, Chen H, Hoffman R W and Angus J C 1990 *J. Mater. Res.* **5** 2378
[64] Egerton R F 1986 *Electron Energy Loss Spectroscopy in the Electron Microscope* (New York: Plenum)